Observations of a Tropical Thunderstorm Using a Vertically Pointing, Dual-Frequency, Collinear Beam Doppler Radar

P. B. CHILSON, C. W. ULBRICH, AND M. F. LARSEN

Department of Physics and Astronomy, Clemson University, Clemson, South Carolina

P. PERILLAT

National Astronomy and Ionosphere Center, Arecibo, Puerto Rico

J. E. KEENER

Department of Physics and Astronomy, Clemson University, Clemson, South Carolina

(Manuscript received 20 July 1992, in final form 19 January 1993)

ABSTRACT

This paper describes an investigation of a thunderstorm that occurred in the summer of 1991 over the National Astronomy and Ionosphere Center in Arecibo, Puerto Rico. Observations were made using collinear dual-wavelength Doppler radars, which permit virtually simultaneous observation of the same pulse volume using transmission and reception of coherent UHF and VHF signals on alternate pulses. This made it possible to directly measure the vertical wind within the sampling volume using the VHF signal while using the UHF signal to study the nature of the precipitation. The observed storm showed strong similarities with systems observed in the Global Atmospheric Research Program's Atlantic Tropical Experiment study. Since this experiment can determine the various microphysical parameters, such as the vertical air velocity, the mean fall speeds of the precipitation, and the reflectivity, the relationships between these parameters that have been postulated in past studies can be tested. For example, in this paper, the method of using reflectivities to deduce the fall speeds of precipitation particles is studied. The method is found to be unreliable when used in turbulent environments.

1. Introduction

The purpose of this work is to describe the preliminary results from a dual-wavelength Doppler radar system that was used to acquire observations of a tropical thunderstorm cluster. When single-frequency Doppler radar is employed in the investigation of cloud and precipitation microphysics, one must make the compromising decision as to which wavelength to use. Frequencies optimal for the study of precipitation are extremely insensitive to motions of the air through which the precipitation is moving. In choosing a wavelength that can detect the air motion, a limit has been placed on the range of precipitation particles that can be observed. The observations to be discussed in this work, however, are unique in that the dual wavelengths used enable a virtually simultaneous determination of both the vertical air motions and the precipitation fall speeds. Data obtained from a UHF (430 MHz) Doppler radar were used in the investigation of the precipitation, while a VHF (46.8 MHz) Doppler radar was used to determine the extent of the vertical motion of the air. Methods used in the analysis of the data for determining the storm's vertical winds and physical parameters related to precipitation particle size are described.

One of the most critical parameters deduced from such measurements, and one of central importance in cloud and precipitation microphysics, is the distribution of the water particles as a function of diameter $N(D)$. The drop size distribution (DSD) has been shown to be well approximated by a gamma distribution (Ulbrich 1983; Deirmendjian 1965) of the form

$$N(D) = N_0 D^{\mu} e^{-\Lambda D}, \tag{1}$$

where $N(D)$ is the number of raindrops of diameter D per unit volume per unit diameter interval and N_0, Λ, and μ are parameters of the distribution. To find the DSD accurately from Doppler radar spectra it is necessary to have accurate measurements of the particle fall speeds, which in turn requires that accurate estimates be made of the motion of the air through which the drops are falling.

Corresponding author address: Dr. Phillip B. Chilson, Department of Physics and Astronomy, Kinard Laboratory of Physics, Clemson University, Clemson, SC 29634-1911.

© 1993 American Meteorological Society

Single-frequency Doppler radars for the observation of clouds and precipitation systems at vertical incidence have been employed by many investigators. Early work includes that of Caton (1966) and Battan and Theiss (1970). Each of these investigations suffered from a severe restriction, namely, an inability to unambiguously determine the magnitude of the vertical wind. In single-frequency Doppler radar studies, a time series of backscattered signals from the falling raindrops is converted to a Doppler velocity spectrum through a Fourier transform, but this will not yield the true motion of the particles. The drop velocities determined in this way are biased by the presence of any vertical wind. To find the true terminal fall velocities that the particles would experience in a quiescent medium, the vertical wind must be removed.

A method of correcting for vertical wind was devised by Rogers (1964), who found a theoretical relation between the mean Doppler fall speed $\langle v_f \rangle$ and the reflectivity factor Z. The measured value of Z is used in this relation to find $\langle v_f \rangle$, which is then subtracted from the measured mean Doppler velocity $\langle v \rangle$ to find the vertical wind. The latter value is then subtracted from each of the Doppler velocities in the spectrum, thus yielding the actual fall speeds of the particles from which their sizes can be found. Since Rogers' work, many empirical relations of similar form have been suggested in an effort to improve the accuracy of the method, such as the work of Joss and Waldvogel (1970), Willis (1984), and others.

The importance of including the vertical velocity corrections was demonstrated by Atlas et al. (1973), who showed that estimates of the drop size distribution deduced from the Doppler spectrum were extremely sensitive to errors in the determination of the vertical wind. In fact, they found particle concentrations to be in error by orders of magnitude resulting from errors in the determination of the vertical wind of only 0.25 m s^{-1}. Therefore, the usefulness of vertical incidence measurements and empirical relations similar to that proposed by Rogers (1964) was said to be limited to those cases where the vertical winds were small and relatively uniform, such as in stratiform rain. A turbulent medium can also corrupt the Doppler velocities associated with the water particles. The precipitation particles are carried along with the turbulence, which has the effect of "smearing" their backscattered signal across the frequency bins in the Doppler spectrum. This in turn broadens the spectrum, which leads to an erroneous assessment of the actual diameters of the particles and their distribution function.

Other methods of analysis have been proposed for extracting the vertical wind from the Doppler spectrum. Hauser and Amayenc (1983) and Klaasen (1989) have attempted to deduce the vertical wind, not by direct measurement, but through analysis methods based on changes in the structure of the Doppler spectrum produced by the presence of updrafts or downdrafts. Still other methods have been devised that try to identify some feature in the spectrum that can be attributed to the vertical air motion. The work of Dennis (1990) shows a signature in the spectrum attributed to the presence of lightning in the radar sampling volume, presumably due to the radar's ability to detect the ionized plasma created by the lightning. If the plasma is carried along with the vertical wind and if the characteristic signature can be spotted in the spectrum associated with the sampling volume, then the vertical air motion can be deduced. The approach provided a very limited number of times and heights in which the vertical wind could be estimated, namely, only those times when lightning was present and could be identified in the sampling volume. It is sometimes possible to isolate the vertical wind contribution from the precipitation contribution in the Doppler spectrum in the case where the contributions from the two are well separated in velocity (Gossard and Strauch 1988; Gossard et al. 1990, 1992; Wagasugi et al. 1986, 1987). This is normally possible only for a limited range of altitudes and usually only when the rainfall rate is large. In a study with the same general goals as the ones described here, Currier (1990) has used two different vertically pointing Doppler radars with frequencies of 50 and 915 MHz for his investigation of precipitation. However, there was an uncertainty introduced in his investigation due to the fact that the two radars were not collinear.

2. Theoretical background

The backscattered power received by a radar antenna is related to the total transmitted power through the radar equation. For a Gaussian beam pattern, the radar equation in the far field can be expressed as (Battan 1973)

$$\bar{P}_r = \frac{c}{1024\pi^2(\ln 2)} (P_t \tau \lambda^2 G^2 \theta \phi)\left(\frac{\eta}{r^2}\right), \qquad (2)$$

where $\bar{P}_r$ (W) is the average returned power, P_t (W) is the transmitted power, c (m s^{-1}) is the speed of light, τ (s) is the pulse duration, λ (m) is the radar wavelength, G is the antenna gain, θ and ϕ are the 3-dB beamwidths, η (m^{-1}) is the reflectivity per unit volume, and r (m) is the range. The scattering mechanisms to be considered here are the precipitation particles (precipitation contribution) and the spatial variations of the refractive index of air (turbulent contribution). Assuming a collection of spherical scatterers in the Rayleigh approximation (dimension of the particles smaller than $\lambda/10$), then

$$\eta = \frac{\pi^5}{\lambda^4} |k|^2 \sum_{i=1}^{n} n_i D_i^6 = \frac{\pi^5}{\lambda^4} |k|^2 Z \times 10^{-18}, \qquad (3)$$

where $|k|^2$ is the refractivity factor, n_i (m^{-3}) is the concentration of particles of diameter D_i (m), and Z

($mm^6\ m^{-3}$) is defined as the radar reflectivity factor with the sum running over all particles within the sampling volume. For water, $|k|^2$ is approximately equal to 0.93 and for ice it is approximately 0.21. When an inertial subrange extends to wavelengths equal to half the radar wavelength λ, turbulent fluctuations in the refractive index produce a turbulent reflectivity that can be expressed as

$$\eta = 0.38\lambda^{-1/3}C_n^2, \tag{4}$$

where C_n^2 is the structure constant that parameterizes the intensity of refractivity turbulence. Also, C_n^2 is directly proportional to the mean-square fluctuations of the refractive index $\langle \Delta n^2 \rangle$ and the outer scale of the turbulence.

Larsen and Röttger (1987) have discussed the contributions of the two reflectivity factors to the backscattered power at UHF and VHF frequencies. In Fig. 1 the reflectivities for turbulent scatter and for precipitation are shown as a function of the radar wavelength. The plotted values correspond to $Z = 30$ and 50 dBZ and are typical of those observed in moderate and heavy rainfall, respectively. The values of C_n^2 equal to $10^{-15}\ m^{-2/3}$ and $10^{-13}\ m^{-2/3}$ are likewise representative of what one might find in moderate and severe turbulence similar to that expected in a thunderstorm. It is clear that the returned signal at UHF (70 cm) will be dominated by precipitation, whereas VHF (6 m) should exhibit some contribution from both precipitation as well as turbulence. It is this property that makes VHF a suitable frequency for obtaining the vertical air velocities, even in the presence of precipitation.

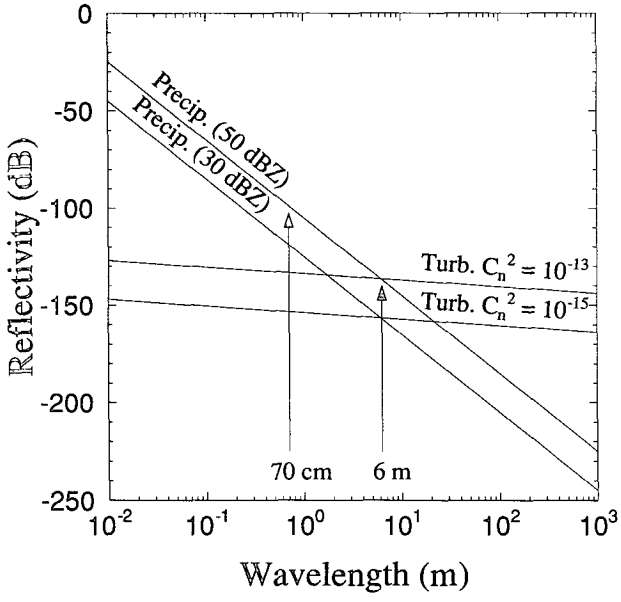

FIG. 1. Plot of reflectivity η as a function of radar wavelength λ for precipitation and clear-air turbulence. The values of Z (dBZ) and C_n^2 shown are typical of those found in a thunderstorm environment. The wavelengths used in this experiment are indicated.

The VHF spectra are also useful in deconvolving the effects of turbulence from the precipitation (or UHF) spectra. As mentioned above, the presence of turbulence has the effect of broadening the spectrum of Doppler velocities. Wagasugi et al. (1986) have discussed how the precipitation spectra might be affected by a turbulent environment. With a DSD as given in Eq. (1), one expects a normalized Doppler spectrum due to precipitation $S_1(v)$ to be given by

$$S_1(v)dv = \frac{D^6N(D)dD}{Z}, \tag{5}$$

where v is the vertical Doppler velocity (in this case, the terminal fall speed of the precipitation particles). This is the expected spectrum for a quiescent environment. If one assumes that the turbulent velocities of the air through which the raindrops are falling have a Gaussian distribution, then the normalized spectrum from the air return will be written as

$$S_2(v) = \frac{1}{(2\pi\sigma^2)^{1/2}} \exp\left(\frac{-v^2}{2\sigma^2}\right), \tag{6}$$

where σ is the variance. The spectrum of Doppler velocities actually observed consists of $S_1(v)$ convolved in velocity space with $S_2(v)$ as well as a contribution from $S_2(v)$ alone. When the magnitude of the vertical wind w is included, the form of the observed spectrum S_0 is obtained,

$$S_0(v) = P_1S_1(v - w) * S_2(v) + P_2S_2(v - w), \tag{7}$$

where P_1 and P_2 are the backscattered powers from the precipitation and turbulence, respectively. Here the convolution is shown by the asterisk operator. This form of the equation does not take into account any system errors or beam-broadening effects. Wagusuki et al. (1986) describe a windowing function $W(v)$ that can be introduced to take into account the truncation of data. Based on the results of Larsen and Röttger (1987) as discussed above, one would expect P_1 to be much larger than P_2 for UHF, and P_1 and P_2 to be of comparable magnitude for VHF.

The DSD, $N(D)$, and the mean Doppler precipitation particle fall speed $\langle v_f \rangle$ can be calculated from the observed normalized Doppler spectrum. The fall speed v_f is given by $v_f = v - w$. If the effects of turbulence are removed, the DSD can be found from Eq. (5) with the substitution of v_f for v. As can be seen in Eq. (5), v_f must be known as a function of the diameter. This information cannot be determined directly with remote sensing techniques, such as radar probing, and introduces a considerable uncertainty in the determination of the DSD. Such a priori information need not be introduced, however, in the calculation of the mean Doppler fall speed. If a reflectivity weighted mean is

used in making this calculation, the equation has the form

$$\langle v_f \rangle = \int_0^\infty v_f S(v_f) dv_f, \tag{8}$$

which does not take into consideration any data truncation. The radar is not sensitive to the full range of fall speeds; therefore, in reality the limits on the integral are $v_{t\min}$ and $v_{t\max}$, where $v_{t\min}$ and $v_{t\max}$ are the minimum and maximum detected speeds, respectively. As will be discussed in the following, the mean Doppler fall speed can be related to other observables.

3. Description of the experiment

The facilities at the NAIC (National Astronomy and Ionosphere Center) Observatory in Arecibo, Puerto Rico, permit the transmission and reception of coherent UHF and VHF signals on alternate pulses using a collinear feed arrangement. By operating the radar in a vertical orientation using the two frequencies in conjunction, it is possible to virtually simultaneously obtain information from a sampled volume of space relating to its moisture content as well as the vertical wind and the turbulence.

The UHF (430 MHz) and VHF (46.8 MHz) antennas at the Arecibo Observatory share the same 300-m-diameter dish. These antennas are mounted on a platform that is suspended 265 m above the base of the dish. The two yagi antennas used by the VHF system are symmetrically spaced on either side of the 29.3-m line feed used by the UHF system. The fact that the two antennas are coaligned allows the sampling of nearly the same volume of space. Keener et al. (1991) discuss the application of the Arecibo UHF–VHF radar in the analysis of velocity–azimuth display (VAD) data for clear air. Their analysis shows the two systems to be in good agreement up to about 12 km where the VHF data became noisy. The range of heights sampled in this analysis was from 4.5 km up to 18.6 km MSL divided into 48 gates. All references to heights in this work will be expressed relative to mean sea level. Both radars used a 2-μs pulse length giving a range resolution of 300 m. It was not possible to make observations below the 5-km height due to the design of the transmit–receive switch.

Each radar used an interpulse period of 1 ms. After transmission and reception of a code pulse and complementary code pulse at one frequency, the same was performed for the other frequency, giving an effective interpulse period of 4 ms. Since the UHF frequency is approximately nine times larger than the VHF frequency, it was necessary to perform nine times more coherent integration of the VHF signal to produce approximately the same Nyquist velocity as obtained from the UHF signal. To obtain the Nyquist velocity of 22 m s^{-1} used in the analysis, 2 coherent UHF and 18 coherent VHF integrations were done. In order that the two frequencies span the same time interval, thus allowing for valid comparison of the two returned signals, an additional 9 incoherent integrations were done on the UHF data to form a single block data. Since 64-point fast Fourier transforms (FFTs) were used in the analysis, each block corresponds to 4.6 s of real-time data.

In comparing the spectra obtained, it is important to note that the peak transmitted power of the UHF radar is 2.5 MW whereas it is only 50 kW for the VHF radar. Since the UHF transmitter was operated at 75% maximum power and both transmitters used a duty cycle of 0.1%, the average powers of the UHF and VHF transmitters were 1875 and 50 W, respectively. This corresponds to a difference of 15.7 dB. Therefore, the VHF spectra tend to be noisier than the UHF spectra. This can make the extraction of the clear-air signal from the spectra in the higher altitudes difficult at times. Another difference in the two systems is the distance to the far field. The antenna gain appearing in Eq. (1) has been given by Stutzman and Thiele (1981) to be

$$G = \frac{4\pi A_e}{\lambda^2}, \tag{9}$$

where A_e is the effective aperture. This equation is valid in both the near and far field with the range dependence lying in A_e. In the far field the equality exists $A_e = A$, where A is the actual illuminated diameter of the dish. In the near field, however, the effective aperture is given by (Farley 1983)

$$A_e = \frac{\lambda^2 r^2}{A}, \tag{10}$$

where r is the range. Therefore, the returned power should drop off as r^{-2} in the far field but show no r dependence in the near field. Farley further states that the distance to the far field is roughly 1–2 D^2/λ, where D is the effective diameter of the dish and λ is the radar wavelength. For both the UHF and VHF systems the illuminated diameter is 200 m. This would put the far field between 57 and 114 km at UHF and between 6.5 and 13 km at VHF. Comparison of the returned powers of the two radar systems in clear air seems to suggest that the VHF far field begins at about 8.1 km (gate 13). Clearly all observations are made in the near field at UHF, but the transition occurs within the bounds of the data to be considered at VHF.

4. Measurements

The data presented here were obtained as a convective thunderstorm passed over the Arecibo observatory on 21 August 1991. A sounding at the San Juan airport (90 km to the east) taken 3–4 h after the data collected in this experiment shows a very moist atmosphere at all levels and a Showalter stability index of −2.3, indicative of the potential for strong thunderstorm ac-

tivity. Light winds were blowing from the east ($\simeq$4 m s^{-1}) in the lower levels with a layer of 12 m s^{-1} easterlies at altitudes of 2.5–4 km. Above a height of about 12 km the winds reverse direction and are generally west-northwest at about 6 m s^{-1}. This reversal of wind direction produces shear, which will be quite evident in the time–height cross sections to be presented later in this work.

The data collected on 21 August span the period from 1400 to 1629 LST. Light and intermittent rain was observed on the ground initially, but the radar data for this period are not shown here. A time–height cross section of data collected from 1453 to 1626 LST is given in Fig. 3 as an illustration of the development of the storm, but the main focus of this work will concentrate on those data taken beginning at 1545 LST during the most dynamic activity. The data from the lowest gates are not shown due to the high levels of noise from the transmit–receive switch. This is likewise true in subsequent figures. At 1550 LST frequent lightning events and heavy rain began to be observed over the radar and persisted, except for a brief decrease in storm intensity at 1622 LST. At 1629 LST a lightning strike caused a power outage at the facility and disabled the compressor servicing the receiver, which forced a discontinuation of the observations. Heavy rain continued to be observed at the ground for at least an hour after the power outage.

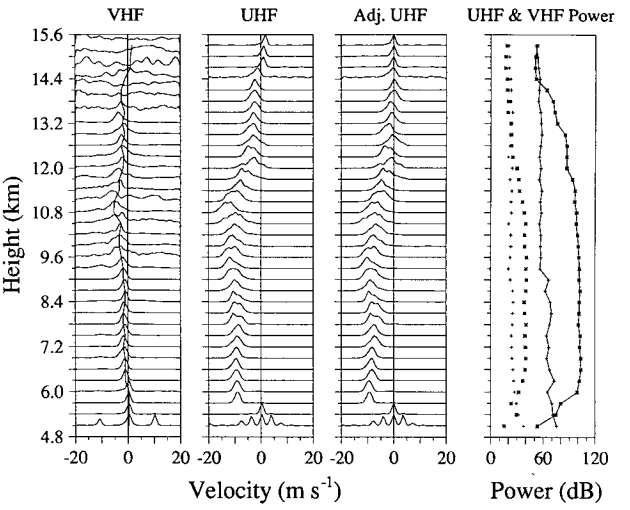

FIG. 2. An example of the display used in determining the vertical winds from the UHF and VHF spectra. Each spectrum has been normalized to its peak value and is displayed on a linear vertical scale. The VHF spectra are given in the first column along with a solid curve showing the estimation of the vertical wind. Both the UHF spectra and the adjusted UHF spectra (with vertical winds subtracted) are shown in the second and third columns, respectively. In the power and noise profiles, the UHF values are given by asterisks and the VHF values by plus signs. The symbols connected by line segments denote the power, whereas those not connected indicate the noise level.

5. Determination of the vertical wind

As stated in section 4, the sensitivity of the VHF radar to turbulent scatter makes it the logical choice for extracting the vertical winds from the spectra. When there is sufficient power in the returned signal from the VHF radar, the updrafts and downdrafts can be readily identified. If the returned signal from the turbulence is significantly greater than that from the precipitation, then the turbulent contribution will be dominant. In such cases there is a clear advantage to the dual-frequency method over the single-frequency method since a large separation in velocity need not exist in order to study the winds and the precipitation. The winds are obtained from the VHF radar and the UHF radar is used to analyze the precipitation. It was often the case for the VHF data, however, that either the signal was too noisy, especially in the upper gates, or the precipitation signal overshadowed the turbulent scatter signal. In these instances, one can examine the UHF spectra to try and pick out the wind. Although the UHF radar is rather insensitive to smaller precipitation particles, they are often present within the sampling volume in great enough numbers to enable detection. If one assumes that these lighter particles are instantaneously carried along with the wind, then they will act as tracers. Thus, a small contribution that can be attributed to the clear-air return can be seen in the UHF spectrum.

An example of the data obtained at 1510 LST (early in the development of the storm) is given in Fig. 2. The spectra shown here are displayed using a linear power spectral density scale, and a three-point running average has been performed to smooth the spectra. Since these data have all been normalized to the peak in each spectrum, the corresponding power is also displayed for reference on the right side of the figure. The UHF power and noise are given by the connected and separated asterisks, respectively. The VHF power is likewise shown using plus signs. It should be noted at this point that the radar has not been calibrated in the troposphere and any powers given in this discussion will be relative powers. For these data, five blocks were incoherently integrated corresponding to 25 s of real-time sampling. A line has been drawn through the VHF data to show which peaks were used in deducing the vertical wind. Here the positive Doppler velocities correspond to motion away from the radar. Since the power in the VHF signal begins to decrease as r^{-2} after gate 13, the spectra begin to get progressively more noisy. From the power profile given in Fig. 2, it is seen that the returned power in the UHF signal begins to decrease rapidly above 14 km, due to the presence of the tropopause at that height, which inhibits the development of the storm to higher altitudes. Above the tropopause, the UHF spectra are used to determine the vertical wind since any precipitation particles above those altitudes will be small. The adjusted UHF spectra

are also given in Fig. 2. Here the vertical wind has been removed from the spectra giving the Doppler velocities that would be produced by the terminal velocities of the water droplets alone. The effects of turbulent broadening are still present since no deconvolution has been performed. This will not, however, affect the estimate of the vertical wind since any convolution will broaden the spectrum but not shift the peak.

The 93 min of data taken as the storm passed over the observatory have been divided for analysis. The first 53 min of the data corresponding to the early development of the storm consist of 65 data segments. Each data segment was constructed from ten incoherently integrated blocks or 50 s of real-time data. The remainder of the data was divided into 100 data segments using five incoherently integrated blocks. During these time intervals, vertical wind profiles were generated for each data segment. To minimize the possibility of falsely labeling a peak in the spectrum as a clear-air peak, the following procedure was used. The normalized UHF and VHF data were overlapped on the same axis for comparison over a range of gates. The first data segment was examined closely to determine the magnitude of the vertical wind. Then the vertical wind profile that was generated and the UHF spectra with the vertical winds removed were displayed. If any abrupt changes occurred from gate to gate, then the UHF–VHF data were reexamined. In picking out the vertical wind from the next data segment, the same approach was used but, in addition, the data from the previous data segment were considered. Here an attempt was made to prevent any abrupt changes in the vertical wind profiles and adjusted UHF spectra both from gate to gate as well as from data segment to data segment. In regions where the VHF data seemed noisy or otherwise unreliable, the UHF data were used. In this way the confidence level in the assessment of the vertical wind profiles was increased.

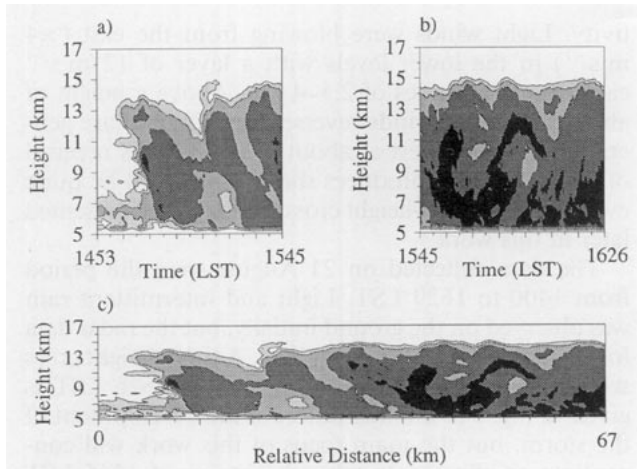

FIG. 3. Time–height profile of UHF relative power showing the cross section of the storm as it passed over the radar. Shown are the 90-, 100-, 110-, and 120-dB contour levels in relative units. The darker shading represents larger values. The distance shown along the abscissa in (c) is calculated assuming the storm is moving horizontally at 12 m s^{-1}.

6. General features of the storm

Since all observations made with the UHF radar are in the near field, the reflectivity of the precipitation aloft will be directly proportional to the power calculated from the Doppler spectra as given by Eqs. (2), (9), and (10). Although the radar is uncalibrated, the relative power obtained will translate into actual power through a linear relationship. Furthermore, since the UHF radar is operating in the near field and there is no r^{-2} dependence, the power is also directly proportional to the reflectivity Z. Again there is no calibration, but any scaling factor in the values of Z will simply be present as a constant additive factor when displayed logarithmically. A time–height cross section of the UHF power is shown in Fig. 3 corresponding to the time when the storm first passed over the radar till the point of the power outage. The main activity of the storm is present within the last 40 min of the data and is shown in Fig. 3b. In both Fig. 3a and Fig. 3b, the abscissa has been divided into roughly 3-min increments. Contour levels are in arbitrary units with the minimum contour level corresponding to a value of 90 dB increasing to 120 dB in 10-dB increments. With the exception of a precipitation-producing cell extending to a height of about 8.7 km at 1418 LST, there was very little activity prior to the onset of the storm at 1500 LST where cloud top is seen to extend to the tropopause. From the soundings taken at the San Juan airport, the winds at the 700-mb level are 12 m s^{-1} and out of the east-southeast. Taking this as the rate at which the storm is advancing, the corresponding horizontal extent of the data would be 67 km and the vertical extent is 12 km. Figure 3c shows the storm using this scale.

One of the notable features of the storm as seen in Fig. 3 is the tilted columns of high returned power. Early in the storm the tilted columns correspond to the progression of raindrops falling through the cloud. The droplets begin forming and become detectable in the spectra near the top of the cloud at roughly 13.5 km. At later times there is a distinct height representing a boundary of precipitation sweeping through the cloud. Above the interface one can identify a precipitation peak in the UHF spectra that is not present in the lower sampled heights. This is particularly noticeable from 1515 to 1520 LST as a steep gradient in the UHF power. The precipitation boundary itself advances through the cloud at a rate consistent with the average fall speed of the precipitation particles, or roughly 4 m s^{-1}. The vertical motion of the particles together with the horizontal motion of the storm cause the tilted structure in the UHF power. As time progresses, a region in the storm begins developing wherein

the tilt of the columns changes orientation and they become tilted in the opposite direction (see, e.g., Fig. 3b). This will be seen to be attributed to the strong vertical updrafts that form as the storm intensifies and to the vertical shear in the environmental winds.

Two time–height cross sections of the vertical wind corresponding to the data in Fig. 3b are shown in Fig. 4. It can be seen in Fig. 4b that the updrafts dominate this region of the storm. Although only the 6, 12, and 18 m s^{-1} contour levels are indicated, the updrafts reach magnitudes greater than 22 m s^{-1}. Shown in Fig. 4c and 4d are the UHF power along with a profile of the horizontal wind. The profile shows the component of the wind parallel to the propagation of the storm with the negative velocities indicating the storm's direction of travel. The vertical winds are primarily upward in this region of the storm with downdrafts becoming stronger only in the lowest sampled heights with the increase of the flux of rain particles. In contrast, there were few incidents of updrafts in excess of 4 m s^{-1} in any of the earlier data for this day. The majority of the vertical wind activity was in the form of downdrafts of 1–2 m s^{-1}. As the storm intensifies, however, regions of strong updrafts begin to form increasing in both size and magnitude with time. The incidence of these cores of vertical winds occurs in pulses corresponding to a series of convective cells. This is indeed what one would expect at the leading edge of a tropical disturbance initiated by a wave (Houze 1977). A periodicity can also be seen in the structure of the precipitation before the development of the convective cells.

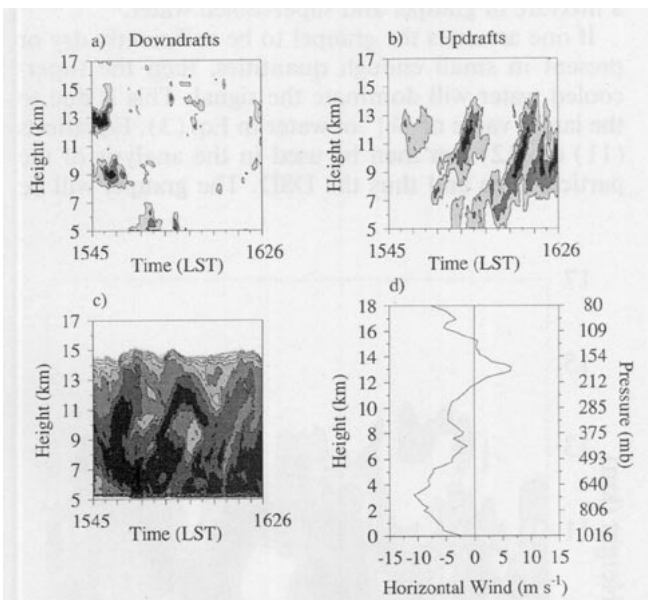

FIG. 4. Time–height profiles of the vertical winds [(a) and (b)], with the corresponding UHF power profile (c), and horizontal wind sounding determined from a radiosonde released at San Juan. The −2 and −6 m s^{-1} downdraft contours are shown in (a) and the 6, 12, and 18 m s^{-1} updraft contours are shown in (b). An averaging algorithm has been used to smooth the data for the sake of presentation. Each element of the data array used in the contouring routine was averaged with the weighted values of the four adjacent array elements. A weighting factor of one-fourth was used. In (c) the UHF power is shown with the contour levels range from 90 to 120 dB increasing by 5 dB. Shown in (d) is the component of the horizontal wind that is parallel to the storm's direction of travel (east-southeast), with negative values representing the forward motion.

Although the tropical wave that passed over San Juan was relatively mild, it was sufficient to produce thunderstorms and heavy rain. Reed and Recker (1971) reported a strong correlation between the passage of tropical waves and the development of mesoscale convective systems (MCS). Houze and Betts (1981), in a review of the Global Atmospheric Research Program's Atlantic Tropical Experiment (GATE), state that nonsquall cloud clusters formed ahead of the trough and moved slightly more slowly than the phase speed of the wave, whereas squall clusters formed ahead of the trough and moved at roughly twice the speed of the wave. Nevertheless, the two phenomena show striking similarities. In both cases, the leading edge of the line is characterized by discrete line elements (LEs) of convective cells. Each LE will rapidly grow to heights penetrating the tropopause. The onsets of the LEs are also accompanied by gust fronts creating strong updrafts. All of these features are evident in the data obtained from the storm in the present work.

7. Fall speeds of the precipitation particles

After determining the magnitude of the vertical wind, the UHF spectra can be adjusted to correspond to those Doppler fall speeds that would be measured in a stationary medium. Since the effects of turbulent smearing have not been removed in the present analysis, some broadening of the spectra will be included. Moreover, it is useful in the analysis of terminal fall speeds to correct for the differences in density of the medium. Foote and du Toit (1969) have studied the effects of the ambient pressure on the drag coefficient of water particles falling through air and have reported a dependence on fall speed to density of the form $(\rho_0/\rho)^{0.4}$, where ρ is the air density aloft and ρ_0 is the air density at some reference level. That is, the terminal fall speeds observed aloft v_f can be related to those that would be measured at ground level through this scaling factor. Although this correction has become the standard, Beard (1985) states that this empirical equation was obtained from particles that had not obtained their terminal velocities. He suggests an adjustment to the velocities as given by $(\rho/\rho_0)^{0.45}$ for heavy rain to be more appropriate. As seen in Fig. 5, there is little deviation between the two adjustments at lower altitudes, but at 15 km the two differ by 10%. The latter relation will be used in this work for relating the fall speeds of all particles to the 1013-mb level.

Figure 6 shows a time–height contour of the mean Doppler fall speeds of the precipitation particles for the same time span as given in Figs. 3a and 4. It should

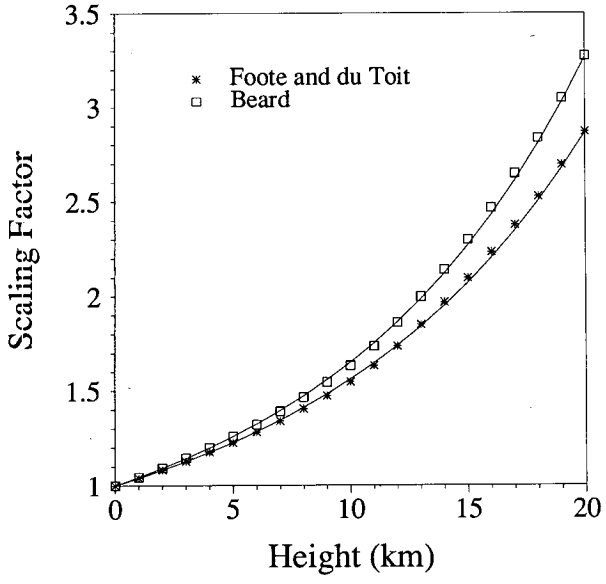

FIG. 5. A plot of the scaling factor correction to the fall speeds of precipitation particles aloft as given by Beard (1985) and Foote and du Toit (1969).

be noted that the average fall speeds shown in Fig. 6 reach a maximum value of roughly 9 m s^{-1} in the regions of convective activity. Although all observations were made above the freezing level, the convective uplift would be sufficient to carry significant quantities of supercooled water into the higher elevations. Leary and Houze (1979) assert that the heavily rimed graupel particles observed in the anvil of a convective tropical storm supports this assumption. That supercooled water is present at these altitudes and that average fall speeds are below the 9.65 m s^{-1} limit established by Gunn and Kinzer (1949) lend further confidence to the method of extracting the vertical winds.

Both Figs. 4c and 6 reveal a peculiar feature near 1607 LST. A depression occurs in the figures corresponding to a reduction in the water content in that region. Examination of Fig. 3b further reveals that this vault lies in a region between two of the convective cells. The profile of the horizontal wind shows the majority of the winds to be out of the east-southeast, with the exception of a thin layer of winds at 6 m s^{-1} coming from the west-northwest at a height of 13 km. The jet produces a shearing of the particles being carried aloft by the first cell and carries the moisture over into the next cell. As the precipitation is being transported along horizontally, some of the particles break up in the turbulent environment. Not only can this be seen in the patchy appearance of the UHF power and the mean Doppler fall speeds, but the individual spectra reveal this as well. A bimodal pattern is seen in the spectra obtained from the region over the vault indicative of two distinct distributions of particles.

Once the fall speeds of the precipitation particles have been deduced, it is possible to calculate the actual diameters of the particles. To do this, however, one needs a relationship between v_f and D. The primary factors governing this relationship are particle size and shape and the phase of the particle substance, that is, liquid (sphere, oblate spheroid) or ice (graupel, hail, snow). The Gunn and Kinzer fall speeds of liquid water particles having diameters in the range $0.06 \leq D \leq 0.58$ cm can be very well approximated by the form (Atlas et al. 1973)

$$v_f = 9.65 - 10.3e^{-6D}, \tag{11}$$

with v_f given in meters per second and D in centimeters. Power laws having the form

$$v_f = aD^b \tag{12}$$

are also often used. Values of a and b that have been used in various environmental conditions can be found in Atlas et al. (1973). In trying to determine a fall-speed relation for the data presented here, the problem arises of not knowing whether the radar is observing raindrops, graupel particles, or snow. As stated earlier, all of the data are above the freezing level, but the regions of strong convection are carrying supercooled water aloft. It is believed that the precipitation can best be described as being graupel particles prior to the passage of the LEs. Thereafter the radar backscatter is from a mixture of graupel and supercooled water.

If one assumes the graupel to be sufficiently dry or present in small enough quantities, then the supercooled water will dominate the signal. This is due to the larger value of $|k|^2$ of water in Eq. (3). Equations (11) or (12) can then be used in the analysis of the particle sizes and thus the DSD. The graupel will be

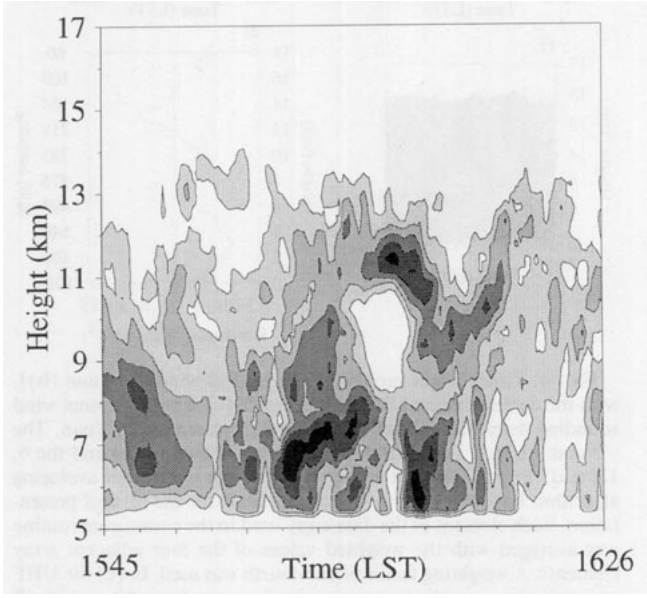

FIG. 6. Time–height contours of the mean Doppler fall speed of precipitation particles. The contour levels range from 3 to 7 m s^{-1} incremented by 1 m s^{-1}. A smoothing algorithm as described in Fig. 4 was used.

the primary source of radar backscatter, however, if it is wet. In this case one must use a power law as given by Eq. (11). Although the values of $\langle v_f \rangle$ all fall below the limit as given in Eq. (11), the turbulence causes many particles to have fall speeds larger than 9.65 m s^{-1}. Therefore Eq. (11) cannot be used for the entire range of fall speeds without employing deconvolution techniques. Nevertheless, the mean Doppler fall speed $\langle v_f \rangle$ can be used with the Gunn and Kinzer equation for calculating the mean particle size assuming supercooled water, since the outliers in the Doppler spectrum will have little effect on the value of $\langle v_f \rangle$. The time–height contours of these values are shown in Fig. 7a with the 1-, 2-, and 3-mm levels shown. For comparison, a similar contour has been generated under the assumption that the radar is observing graupel particles. In Fig. 7b, Eq. (12) has been used with $a = 1.0$ and $b = 0.9$. These values represent an average of the data collected in the National Hail Research Experiment (NHRE) as reported by Heymsfield (1978).

8. The Rogers method

With the knowledge of the magnitudes of the vertical wind and the relative reflectivities, it is possible to test the dependence of the mean Doppler fall speed and the reflectivity used in the Rogers method. Using Eq. (5) along with Eqs. (1) and (12), an expression can be found relating $\langle v_f \rangle$ (m s^{-1}) and Z (mm^6 m^{-3}) through

$$\langle v_f \rangle = \frac{a\Gamma(7+\mu+b)}{\Gamma(7+\mu)} \left[\frac{Z \times 10^{-12}}{N_0 \Gamma(7+\mu)} \right]^{b/(7+\mu)}, \quad (13)$$

where Γ represents the gamma function. The parameters a and b in Eq. (12) are for velocities expressed in meters per second and for particle diameters in centimeters. Equation (13) can be expressed more simply as

$$\langle v_f \rangle = \alpha Z^{\gamma}. \quad (14)$$

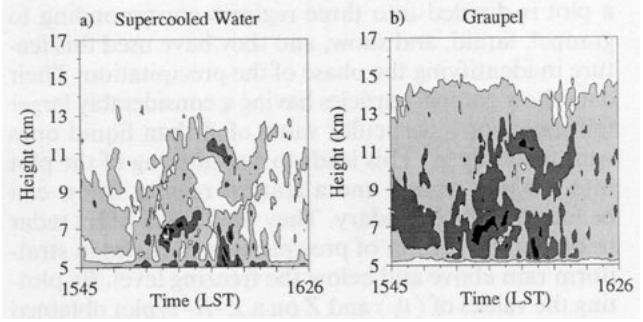

FIG. 7. Time–height profile of precipitation particle sizes calculated from the mean Doppler fall speeds shown in Fig. 6. In (a) it is assumed that the precipitation consists primarily of supercooled water and Eq. (11) was used for the calculation. The values of 1, 2, and 3 mm are contoured. In (b) it is assumed that the returned backscattered power is from graupel particles and Eq. (12) was used with $a = 1.0$ and $b = 0.9$. Shown are the 2-, 6-, and 10-mm contours. A smoothing algorithm as described in Fig. 4 was used.

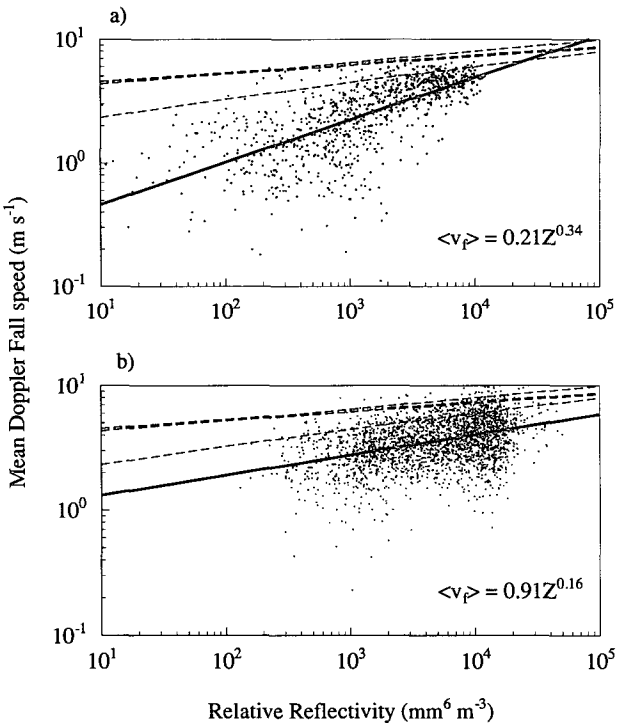

FIG. 8. Log–log plot of mean Doppler fall speeds versus the relative reflectivity. In both plots the fit to the data is of the form $\langle v_f \rangle = \alpha Z^{\gamma}$ and is shown with a heavy line. The upper and lower Joss and Waldvogel bounds (1970) are given by light dashed lines, and the Rogers curve (1964) is shown as a heavy dashed line. Panel (a) corresponds to the data taken during the early development of the storm and (b) is for the convective region.

In his analysis, Rogers (1964) found values of $\alpha = 3.8$ and $\gamma = 0.071$. The relationship was derived assuming a Marshall–Palmer drop size distribution ($\mu = 0$ and $N_0 = 0.08$ cm^{-4}) and fall-speed parameters given by $a = 14.2$ and $b = 0.5$. Joss and Waldvogel (1970) analyzed disdrometer data from seven different storms taken at the earth's surface and found the relationship, $\langle v_f \rangle = 2.6Z^{0.107}$. They were able to fit 68% of the data from each storm within ± 1 m s^{-1} providing upper and lower bounds to the approximation. A discussion of the various forms of Eq. (14) can be found in Atlas et al. (1973).

A plot of the values of $\langle v_f \rangle$ measured in this experiment along with their corresponding values of Z are shown in Fig. 8. An estimate of Z was obtained from the relative reflectivities by assuming a value of $Z = 0$ dBZ above the tropopause. Therefore the Z's in Fig. 8 actually denote the ratios in reflectivities (differences when displayed logarithmically) relative to those measured in the stratosphere. Again the values of $\langle v_f \rangle$ have been adjusted to the 1013-mb level. The data used in Fig. 8a were obtained during the early development of the storm (see Fig. 3a), whereas the data in Fig. 8b represent the region of strong convection (see Fig. 3b). Both the fit to the data (heavy line) as well as the upper and lower bounds from the Joss and Waldvogel analysis

(light dashed lines) have been shown in Fig. 8. In addition, the Rogers relationship (heavy dashed line) is plotted in Fig. 8. The data from both datasets show considerable scatter about the fitted line and little agreement with either the Rogers curve or the bounded values given by Joss and Waldvogel. Whereas the slope of the fitted line in Fig. 8b is similar to those given by Rogers and Joss and Waldvogel, this is not the case for Fig. 8a, where many of the data points are given for smaller fall speeds. The spectral resolution of the velocity is only 0.6 m s^{-1}, making it difficult to determine fall speeds less than about 1 m s^{-1}. Some of the scatter of the data about the fitted line can also be attributed to the effects of lightning in the spectra. A lighting event in the beam will cause fluctuations in the radar time series data, which makes it difficult to extract the peaks associated with the turbulence and the precipitation.

Using the relative values of Z and the mean Doppler velocities, that is, with no corrections for updrafts or downdrafts, the Rogers method has been used to obtain the vertical winds and the mean Doppler fall speeds. In the calculation of $\langle v_f \rangle$, the relationship $\langle v_f \rangle = 2.575Z^{0.033}$ has been used as shown in Fig. 8b. This relationship was chosen (as opposed to one in common usage) to test the method under optimal conditions. The vertical winds were calculated by finding the difference between the mean Doppler velocity and the mean Doppler fall speed. The results are shown in Fig. 9. The vertical winds are shown in Fig. 9a, which shows the general structure of the storm, but the actual magnitudes of the vertical winds have been improperly estimated. Although the three cells can be identified, the peak magnitude of the updrafts is given to be about 13 m s^{-1} compared to the actual peak of more than 22 m s^{-1}. A calculation of the corresponding root mean square (rms) yields a value of 2.98 m s^{-1} using the Rogers method as compared with 6.76 m s^{-1} from the actual data. The rms value of the downdrafts is 1.77 m s^{-1} compared with 1.45 m s^{-1}. In the case of the precipitation fall speeds, the Rogers method yields an rms of 2.54 m s^{-1} compared to the actual value of 3.63 m s^{-1}. The rms values from the Rogers method are considerably worse if the Joss and Waldvogel relationship $\langle v_f \rangle = 2.6Z^{0.107}$ is used. Values of 6.02, 0.81, and 4.32 m s^{-1} are found for the mean Doppler fall speeds, updrafts, and downdrafts, respectively.

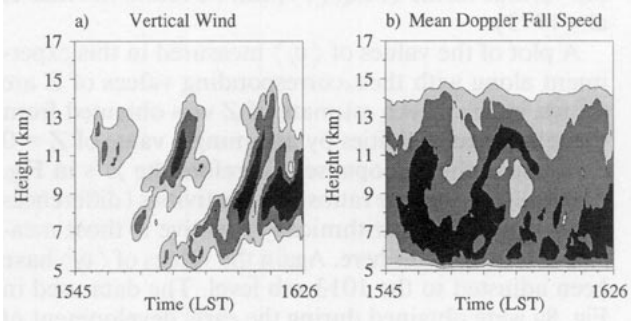

FIG. 9. Contours of the vertical winds and mean Doppler fall speeds as calculated using the Rogers method (1968). In (a) the vertical wind contour levels 3, 6, and 9 m s^{-1} are shown. Panel (b) shows the 2, 3, and 4 m s^{-1} contour levels for the mean Doppler fall speeds. A smoothing algorithm as described in Fig. 4 was used.

The differences between the data obtained in this experiment and the theoretical relationship are not surprising considering several factors. The earlier studies of the dependence of $\langle v_f \rangle$ on Z were conducted at or near ground level. Even then one expects only good agreement for $Z \geqslant 10^4$ mm^6 m^{-3}. Atlas et al. (1973) explain that intense rains measured at ground level consist primarily of larger particles that do not exhibit a wide range of median volume diameters. This seems to be important for the successful application of Z–$\langle v_f \rangle$ relationships. Unfortunately, such an environment is often not found when making measurements aloft. In a study of four different storms, Pasqualucci (1975) used $\langle v \rangle = 2.96Z^{0.095}$ to fit mean Doppler velocities measured at a height of 19 m above the earth's surface to ±0.3 m s^{-1}. At a height of 360 m, however, the data were scattered about the fit by more than ±1.0 m s^{-1}. In a dynamic environment such as found in a thunderstorm, one encounters an inhomogeneous environment resulting in a large variability in the drop distributions. Examination of the individual Doppler spectra reveals considerable structure. Broad and bimodal spectra are often observed, which clearly indicates a large distribution of particle diameters. The tendency of the spectra to possess a bimodal structure is not, however, unique to turbulent environments. Although Gossard et al. (1992) were observing stratiform homogeneous cloud systems, they also report multiple peaks in the spectra corresponding to different particle growth centers.

Another source of error expected in using Eq. (14) is its dependence on the parameters of DSD and the phase of the precipitation particles. In so doing, an assumption of the rainfall rate has likewise been made. Gossard et al. (1992) have proposed the use of a plot relating the reflectivity Z, rainfall rate R, and the Doppler fall speed v_f in the study of precipitation. Such a plot is divided into three regimes corresponding to graupel, liquid, and snow, and they have used this feature in identifying the phase of the precipitation. Their data show graupel particles having a considerably larger fall speed for a particular value of Z than liquid ones with the same Z. This leads to a sectioning of the plot into a liquid regime and a graupel regime. Snow can be found at the boundary. They used a 915-MHz radar to determine spectra of precipitation particles in stratiform rain above and below the freezing level. By plotting the values of $\langle v_f \rangle$ and Z on a Z–R–v_f plot obtained over several range gates, they are able to show a phase transition occurring.

9. Conclusions

In this paper, a thunderstorm associated with a tropical wave was observed as it passed over the NAIC

Observatory in Arecibo, Puerto Rico. The dual-frequency observations of the system made it possible to make direct measurements of the vertical wind as well as to study the nature of the precipitation. This facilitated the removal of the updrafts and downdrafts from the Doppler velocities associated with the falling precipitation particles thus yielding the Doppler fall speeds. An analysis of the data has shown this storm to bear close resemblance to similar systems reported in the GATE studies. Having direct measurements of the mean Doppler fall speeds as well as the reflectivities lead to an analysis of the validity of the Rogers method. Whereas this method can produce the general features of the vertical winds and the mean Doppler fall speeds, it cannot be used reliably to obtain their magnitudes.

Having the ability to directly measure the magnitudes of vertical winds and the precipitation facilitates the study of many aspects of such data. Currently a detailed study of the spectra is being conducted with an emphasis on deconvolving the effects of turbulence from the precipitation signal. This is expected to provide information of the mass flux of the precipitation leading to a better understanding of the particle growth process. An investigation of gravity waves is also under way. Examination of the vertical winds before, above, and after the storm should reveal the atmospheric waves generated by the thunderstorm.

Acknowledgments. The authors wish to thank Robert Palmer for his assistance in the collection and analysis of the data used in this work. This work was sponsored by the National Science Foundation under Grant ATM9003448. The National Astronomy and Ionospheric Center (Arecibo Observatory) is operated by Cornell University under contract with the National Science Foundation.

REFERENCES

Atlas, D., R. C. Srivastava, and R. S. Sekhon, 1973: Doppler radar characteristics of precipitation at vertical incidence. *Rev. Geophys. Space Phys.*, **11**, 1–35.

Battan, L. J., 1973: *Radar Observations of the Atmosphere.* The University of Chicago Press, 323 pp.

——, and J. B. Theiss, 1970: Measurement of vertical velocities in convective clouds by means of pulsed-Doppler radar. *J. Atmos. Sci.*, **27**, 293–298.

Beard, K. V., 1985: Simple altitude adjustments to raindrop velocities for Doppler radar analysis. *J. Atmos. Oceanic Technol.*, **2**, 468–471.

Caton, P. G. F., 1966: A study of raindrop size distribution in the free atmosphere. *Quart. J. Roy. Meteor. Soc.*, **92**, 15–30.

Currier, P. E., 1990: Precipitation measurement using a dual frequency Doppler system. Ph.D. dissertation, University of Colorado, 241 pp. [UMI order number DA9132560.]

Deirmendjian, D., 1965: Complete scattering parameters of polydispersed hydrometeors in the λ0.1 to λ10 cm range. *Radio Sci.*, **69D**, 893–897.

Dennis, T. S., 1990: Analysis of UHF Doppler radar observations of a tropical thunderstorm. Ph.D. dissertation, Clemson University, 150 pp. [UMI order number DEY903417.]

Farley, D. T., 1983: Antenna size for MST radars. *Handbook for MAP*, **9**, S. A. Bowhill and B. Edwards, Eds., SCOSTEP Secretariat, University of Illinois at Urbana–Champaign 465–466.

Foote, G. B., and P. S. du Toit, 1969: Terminal velocity of raindrops aloft. *J. Appl. Meteor.*, **8**, 249–253.

Gossard, E. E., and R. G. Strauch, 1988: Procedural guide for the retrieval of drop-size distributions in water clouds from ground-based clear-air-sensing Doppler radar observations. NOAA/ERL Tech. Document, 44 pp. [NTIS PB 89-152474.]

——, ——, and R. R. Rogers, 1990: Evolution of drop-size-distributions in liquid precipitation observed by ground-based Doppler radar. *J. Atmos. Oceanic Technol.*, **7**, 815–828.

——, ——, D. C. Welsh, and S. Y. Matrosov, 1992: Cloud layer, particle identification, and rain-rate profiles from ZRV_f measurements by clear-air Doppler radars. *J. Atmos. Oceanic Technol.*, **9**, 108–119.

Gunn, R., and G. D. Kinzer, 1949: The terminal velocity of fall for water droplets in stagnant air. *J. Meteor.*, **6**, 243–248.

Hauser, D., and P. Amayenc, 1983: Exponential size distributions raindrops and vertical air motions deduced from vertically pointing Doppler radar data using a new method. *J. Climate Appl. Meteor.*, **22**, 407–418.

Heymsfeld, A. J., 1978: The characteristics of graupel particles in northeastern Colorado cumulus congestion clouds. *J. Atmos. Sci.*, **35**, 284–295.

Houze, R. A., Jr., 1977: Structure and dynamics of a tropical squall-line observed during GATE. *Mon. Wea. Rev.*, **105**, 1540–1567.

——, and A. K. Betts, 1981: Convection in GATE. *Rev. Geophys. Space Phys.*, **19**, 541–576.

Joss, J., and A. Waldvogel, 1970: Raindrop size distribution and Doppler velocities. *Proc. 14th Radar Meteorology Conf.*, Tucson, AZ, Amer. Meteor. Soc., 153–156.

Keener, J., C. W. Ulbrich, M. F. Larsen, M. H. Ierkic, P. Perillat, 1991: Dual-frequency, collinear beam, UHF and VHF radar measurements at Arecibo, Puerto Rico. *Proc. 25th Int. Conf. on Radar Meteorology,* Paris, Amer. Meteor. Soc., 308–310.

Klaasen, W., 1989: Determination of rain intensity from Doppler spectra of vertically scanning radar. *J. Atmos. Oceanic Technol.*, **6**, 552–562.

Larsen, M. F., and J. Röttger, 1987: Observations of thunderstorm reflectivities and Doppler velocities measured at VHF and UHF. *J. Atmos. Oceanic Technol.*, **4**, 151–159.

Leary, C. A., R. A. Houze, 1979: Melting and evaporation of hydrometeors in precipitation from the anvil clouds of deep tropical convection. *J. Atmos. Sci.*, **36**, 669–679.

Pasqualucci, F., 1975: Low altitude Doppler measurements of precipitation at vertical incidence. *Proc. 16th Radar Meteorology Conf.*, Houston, TX, Amer. Meteor. Soc., 415–420.

Reed, R. J., and E. E. Recker, 1971: Structure and properties of synoptic-scale wave disturbances in the equatorial western Pacific. *J. Atmos. Sci.*, **28**, 1117–1133.

Rogers, R. R., 1964: An extension of the Z–R relationship for Doppler radar. *Proc. 11th Weather Radar Conf.*, Montreal, Amer. Meteor. Soc.

Sheppard, B. E., 1990: Measurement of raindrop size distributions using a small Doppler radar. *J. Atmos. Oceanic Technol.*, **7**, 255–268.

Stutzman, W. L., and G. A. Thiele, 1981: *Antenna Theory and Design.* John Wiley and Sons, 598 pp.

Ulbrich, C. W., 1983: Natural variations in the analytical form of the raindrop size distribution. *J. Climate Appl. Meteor.*, **22**, 1764–1775.

Wagasuki, K., A. Mitzutani, S. Fukao, and S. Kato, 1986: A direct method for deriving drop-size distribution and vertical air velocities from VHF Doppler radar spectra. *J. Atmos. Oceanic Technol.*, **3**, 623–629.

——, ——, ——, and ——, 1987: Further discussions on deriving drop-size distribution and vertical air velocities from VHF Doppler radar spectra. *J. Atmos. Oceanic Technol.*, **4**, 170–179.

Willis, P. T., 1984: Relations between mean Doppler velocity and radar reflectivity factor. *Proc. 22nd Conf. on Radar Meteorology,* Zurich, Amer. Meteor. Soc., 338–340.